Scientific Reports

https://doi.org/10.1038/s41598-026-40307-x

Article in Press

Research on stability analysis and control technology of roadways in the underlying isolated island working face

Received: 14 October 2025

Accepted: 11 February 2026

Published online: 19 February 2026

Cite this article as: Gao X., Wang Y. & Li Y. Research on stability analysis and control technology of roadways in the underlying isolated island working face. *Sci Rep* (2026). https://doi.org/10.1038/s41598-026-40307-x

Xiaoxu Gao, Yaowei Wang & Yi-Ming Li

We are providing an unedited version of this manuscript to give early access to its findings. Before final publication, the manuscript will undergo further editing. Please note there may be errors present which affect the content, and all legal disclaimers apply.

If this paper is publishing under a Transparent Peer Review model then Peer Review reports will publish with the final article.

ARTICLE IN PRESS

© The Author(s) 2026. **Open Access** This article is licensed under a Creative Commons Attribution-NonCommercial-NoDerivatives 4.0 International License, which permits any non-commercial use, sharing, distribution and reproduction in any medium or format, as long as you give appropriate credit to the original author(s) and the source, provide a link to the Creative Commons licence, and indicate if you modified the licensed material. You do not have permission under this licence to share adapted material derived from this article or parts of it. The images or other third party material in this article are included in the article's Creative Commons licence, unless indicated otherwise in a credit line to the material. If material is not included in the article's Creative Commons licence and your intended use is not permitted by statutory regulation or exceeds the permitted use, you will need to obtain permission directly from the copyright holder. To view a copy of this licence, visit http://creativecommons.org/licenses/by-nc-nd/4.0/.

ARTICLE IN PRESS

Research on stability analysis and control technology of roadways in the underlying isolated island working face.

Xiaoxu Gao[a], Yaowei Wang[a], Yi-Ming Li[a,b]*

[a]College of Energy and Mining Engineering, Xi'an University of Science and Technology, Xi'an 710054, China

[b]Guangdong Provincial Key Laboratory of Deep Earth Sciences and Geothermal Energy Exploitation and Utilization Shenzhen University, Shenzhen. 518060, China

*Corresponding author

E-mail address: yiming.li@xust.edu.cn

Abstract: The mining of isolated working faces beneath close coal seams is influenced by the overlying goaf, the lateral abutment pressure from adjacent goafs, and the dynamic pressures arising from the preparatory mining operation. The deformation and failure characteristics of the surrounding rock in the roadway show significant variability, especially in sections beneath goaf areas and residual coal pillars, making it difficult to apply a conventional support strategy. This work adopts theoretical analysis, numerical simulations, and field observations to investigate roadway deformation and stability in the underlying isolated island working face according to the geological conditions of the Yanghuopan coal mine in Shaanxi province, China. The results indicates that the stress transfer from the residual pillar beneath the 2^{-2} coal seam influences the 3^{-1} coal seam up to a distance of 62.1 m, with a stress transfer coefficient of 1.6 directly beneath the coal pillar. The vertical stress in the 3^{-1} coal seam is distributed across five distinct regions. The 30119 working face traverses all five regions, with the vertical stress on the coal pillar and surrounding rock deformation reaching their maximum in the regions affected by the concentrated stress of the 1# and 2# residual coal pillars. Stress concentration is significantly reduced beneath the goaf of the 20201 and 20202 panels. Based on these findings, a corresponding stability control scheme was developed. The conventional support zone beneath the goafs and the original rock stress region of the 20201 and 20202 working faces, and the reinforced support zone within the influence of the residual coal pillars.

ARTICLE IN PRESS

Field observations, including surface displacement, anchor forces, and internal coal pillar deformation, validated the effectiveness of the combined support system and ensured safe production during isolated island working face mining.

Keywords: Close coal seams, Isolated island working face, Numerical simulations, Combined support system, Roadway stability, Field monitoring

ARTICLE IN PRESS

ARTICLE IN PRESS

1 Introduction

With the continued intensification of coal resource extraction, maintaining orderly sequencing and rapid turnover of longwall panels has become increasingly challenging in many operations. To reduce mutual interference between adjacent faces and ensure continuous production, the skipping mining method is implemented within the mining region, which resulted in the formation of an isolated island working face[1–3]. Such isolated island-like panels are typically associated with pronounced abutment-stress concentrations, complex overburden structure and enhanced susceptibility to roof separation and dynamic hazards, ultimately impairing roadway serviceability and increasing subsidence-control costs [4,5]. Moreover, when an island panel is extracted beneath an overlying goaf and residual coal pillars, the combined disturbance and stress transfer can substantially degrade pillar integrity and roadway stability, thereby elevating safety risks and necessitating frequent rehabilitation and re-support [6,7].

In recent years, a growing number of works have investigated deformation control and stability management for roadways associated with isolated island working faces in closely spaced seams using theoretical analysis, numerical modeling, and field monitoring [8–14]. In terms of theoretical analysis, Jia et al. proposed the “umbrella arch” overburden structure for the extraction of isolated island panels and derived theoretical formulas for the supporting force required during panel extraction. This approach provided a theoretical understanding of the relationship between the side close to the gob and the side close to the gob in the isolated island panels, as well as the variations in the peak values of the solid coal side elastic response in irregular island panels, both for transportation and return roadways[9]. Yang et al. focused on a typical deep-buried, non-equal width island working face, analyzing the strata structural changes and coal pillar stress evolution caused by the overlying goaf, based on the spatial structure theory of overlying strata[15]. Xue et al. conducted an in-depth study on the layout and support parameter optimization of recovery roadways in thin coal seams with isolated island working faces with theoretical and numerical

ARTICLE IN PRESS

analysis[16]. From a numerical perspective, most researchers have employed the finite element method (FEM) and the discrete element method (DEM) to investigate the deformation of surrounding rock, stress conditions, and failure modes of isolated island panels[17,10,18–24]. Shang et al. and Han et al. employed FLAC3D to conduct in-depth studies on the failure characteristics of surrounding rock in roadways under repeated mining and the mining-induced stress behavior of isolated island panels in closely spaced coal seams[12,18,25]. Wang et al. adopted the ABAQUS to investigate the overburden structure and concentrated pressure control in thick coal seam island longwall panels[11]. Additionally, Wang et al. utilized 3DEC, coupled with micro-seismic monitoring and shockwave CT inversion techniques, to perform detailed research on the dynamic disaster risk of isolated longwall panel extraction. In terms of field observations, Xie et al. employed in-situ measurement techniques to determine the spatial distribution of mining-induced stresses across different sections of the working face, revealing areas of elevated stress concentration beneath the isolated island panel[13]. Huang et al. proposed a roof-breaking blasting pressure-relief strategy. The effectiveness of this approach in mitigating impact hazards was subsequently validated through in-situ borehole peeping and infrared radiation techniques[26]. In terms mechanical mechanism of mining-induced disturbance in coal, several studies have employed the Split Hopkinson Pressure Bar (SHPB) testing to elucidate the dynamic failure properties and energy dissipation of coal samples[27,28]. Zhang et al. and Zou et al. investigated the energy evolution and damage properties of coal subjected to cyclic loading by utilizing the acoustic emission monitoring and CT scan technology[29,30].

Although aforementioned research results provide significant guidance and insights for isolated island working faces, several limitations remain, such as the site-dependent support schemes and challenges in high in-situ stress conditions, etc. Fewer studies systematically quantify the influence on the underlying seam, particularly for vertical arrangements of upper and lower working faces in closely spaced seams. In this work, a theoretical assessment is conducted to delineate the influence range of overlying residual coal pillars on the underlying seam, providing a basis for

ARTICLE IN PRESS

identifying high-risk roadway segments. The comprehensive numerical simulations are further investigated to capture the spatial evolution of stress concentration, plastic failure, and deformation in roadways located beneath isolated island panels, explicitly accounting for the combined effects of overlying goafs and residual pillars. Furthermore, based on the identified deformation characteristics, targeted stability-control schemes are proposed and validated through field observations. The remainder of this paper is structured as follows. First, a comprehensive analysis of the engineering background, stratigraphic characteristics, and surrounding rock mechanical parameters of the Yanghuopan coal mine was presented in Section 2. Then, Section 3 theoretically investigates the influence range of the overlying residual coal pillars on the underlying coal seam. Section 4 presents a comprehensive numerical simulation analysis of the stability of roadways beneath isolated longwall panels in closely spaced coal seams. Some stability control schemes for surrounding rock deformation characteristics are presented and validated with field observations in Section 5. Finally, some conclusions on the proposed combined support systems are presented in Section 6.

2 Case study

2.1. Engineering background

This work focuses on the 30119 working face of the Yanghuopan mine, which is a typical isolated island panel surrounded on three sides by goafs, situated in the 3^{-1} coal seam of the 301 panel. The overlying strata consist of multiple goafs in the 2^{-2} coal seam, including the 20201 and 20202 panels, with an average distance of 29 m between the goaf of the 2^{-2} coal seam. The working face has a width of 240 m and a total advance length of 2225 m. The average coal seam thickness is 2.06 m with an average dip angle of 1°. The mining operation utilizes the fully caving longwall mining method to improve mining efficiency. The research area primarily includes the 30119 working face from 0 to 1150 m, where the working face is surrounded by mined-out areas, forming an isolated island working face.

As shown in Fig. 1, the width of the coal pillar for the main haulage roadways is

ARTICLE IN PRESS

30 m, with 15 m in the return air roadway. The 30119 working face of the Yanghuopan coal mine extends from 0 m to 1150 m along the panel. The roof of this section lies beneath the 2^{-2} coal seam at a vertical distance of 29 m. Specifically, the 0-515 m segment of the working face is overlain by the goaf areas of the 20201 and 20202 working faces in the 202 panel. The 600-1150 m segment is underlain by a fire-affected zone in the 2^{-2} coal seam and associated fire-resistant barrier coal pillars. The roof and floor of the roadway are composed of mudstone. A detailed histogram of the strata is shown in Fig. 2.

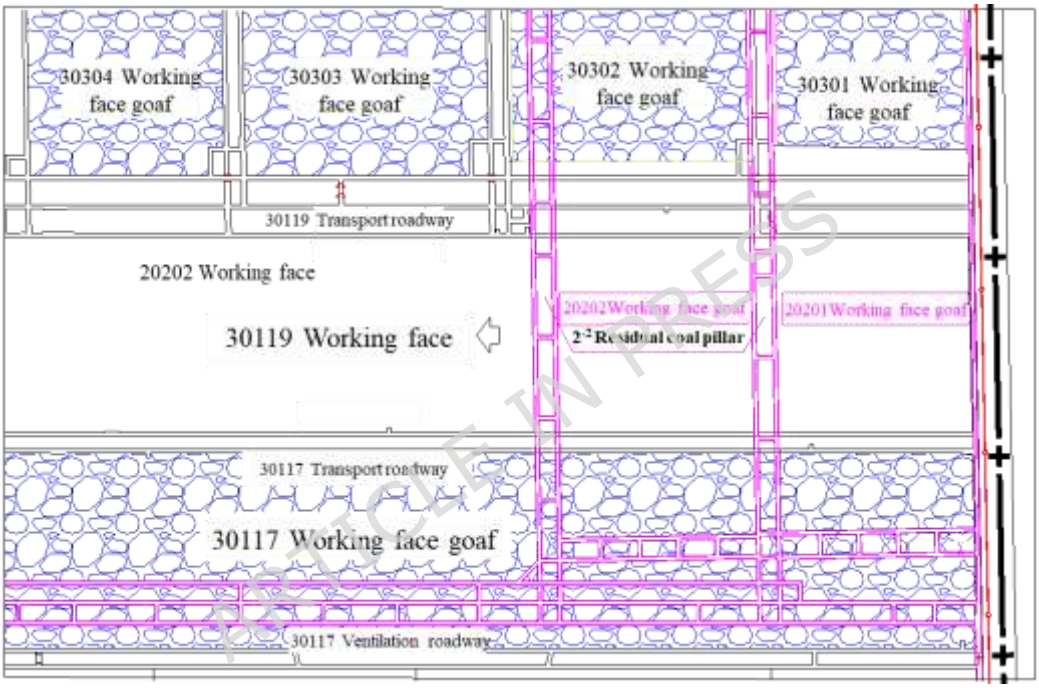


Fig.1 Working face layout.

ARTICLE IN PRESS

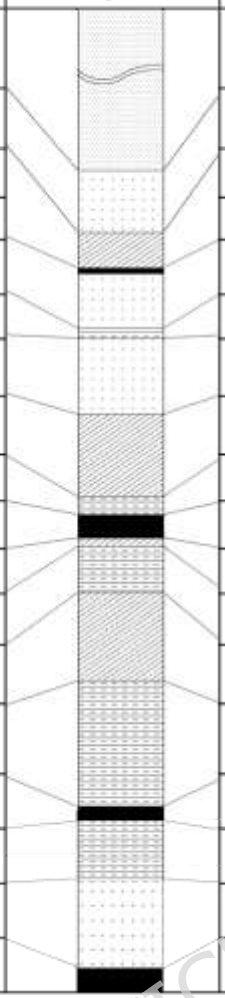
Number	Legend	Depth/m	Thickness/m	Lithologies
1		43.13	43.13	Soil
2		50.83	7.70	Fine-grained sandstone
3		54.95	4.12	Siltstone
4		55.55	0.60	Coal seam
5		62.53	6.98	Siltstone
6		63.88	1.35	Medium-grained sandstone
7		73.28	9.40	Siltstone
8		83.48	10.20	Medium-grained sandstone
9		85.75	2.27	Mudstone
10		88.38	2.63	2^{-2}Coal seam
11		89.43	1.05	Mudstone
12		94.60	5.17	Fine-grained sandstone
13		105.63	11.03	Medium-grained sandstone
14		121.69	16.06	Fine-grained sandstone
15		123.56	1.87	3^{-1}Coal seam
16		125.55	1.99	Fine-grained sandstone
17		135.85	10.30	Siltstone
18		136.57	0.72	3^{-2}Coal seam

Fig.2 Strata formation of the research site.

2.2. Mechanical characteristics of rock samples

To fully understand the mechanical properties of the rock in the isolated island working face of the Yanghuopan mine, some typical laboratory tests (uniaxial compressive strength (UCS), Brazilian tensile strength (BTS) and shear strength tests) were carried out on rock samples(see Table 1). Laboratory test results indicate that the immediate roof of the 3^{-1} coal seam is primarily composed of fine-grained sandstone with a thickness of 16.06m. The average compressive strength, elastic modulus, and tensile strength of the roof siltstone are 54.8MPa, 14.42GPa, and 0.98 MPa, respectively. The rock of the immediate floor is also composed of siltstone, with a thickness of 4.63m, exhibiting an average compressive strength of 61.15MPa, an average elastic modulus of 39.58GPa, and an average tensile strength of 1.31MPa. These mechanical parameters provide critical input for evaluating the stability of the

ARTICLE IN PRESS

roof and floor strata, as well as for developing support strategies in mining operations.

Table 1 Representative parameters of rocks from experimental tests.

Rock types	Compressive strength (MPa)	Young's modulus (GPa)	Cohesion (MPa)	Tensile strength (MPa)	Poisson's ratio	Friction angle (◦)
Roof siltstone	54.8	14.42	2.4	0.98	0.17	39.86
3^{-1}Coal sample	15.4	5.24	0.98	0.48	0.28	36.82
Floor siltstone	61.15	39.58	2.2	1.31	0.32	37.04

3 Theoretical analysis of the effect of the closely overlying residual coal pillars on the overlying coal seam

3.1 Stress transmission law of residual coal pillars in the coal seam floor

During the upper coal seam extraction, partial stress is transferred from the exposed roof strata to the residual coal pillars, which in turn exerts a significant influence on the underlying strata. To facilitate theoretical analysis, the effect of overlying residual coal pillars on the lower coal seam is simplified as a concentrated stress applied at an arbitrary point on the plane of a semi-infinite body. By employing the Lame–Maxwell equations to address the problem of a semi-infinite plane wedge under concentrated loading, it can be demonstrated that the principal stress coordinate system is equivalent to the polar coordinate system, yielding the stress solution for the semi-infinite plane. Treating both the residual pillars and the floor as elastic bodies, and applying the equations for vertical concentrated loading at the pillar boundaries in conjunction with the principle of superposition, the transmission of concentrated stress into the floor can be established.

ARTICLE IN PRESS

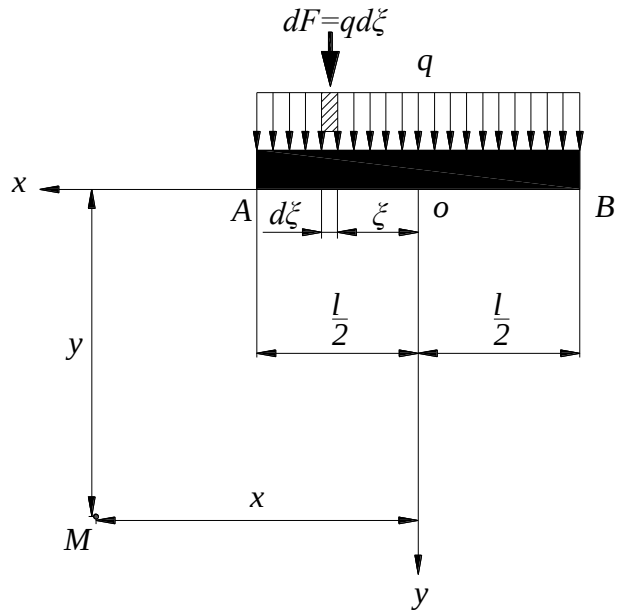


Fig.3 Mechanical model of concentrated stress transfer from residual pillars to the coal seam floor

According to elastic mechanics theory, when a residual coal pillar is subjected to a vertical concentrated load acting along the segment AB at both sides, the finite length of the loaded segment can be represented by an equivalent uniformly distributed line load with intensity *q*. For an arbitrary point M located in the rock mass beneath the floor of the residual pillar, the Cartesian coordinate system is established as illustrated in Fig. 3. Taking the midpoint of AB as the origin O, the point M is located at a horizontal distance *x* and a vertical distance *y* from the origin O, and therefore has coordinates (*x*, *y*). Along the segment AB, at a horizontal distance ξ from point O, a differential element of length dξ is considered, on which an infinitesimal vertical force d*F* acts. The horizontal and vertical distances from point M to the differential force d*F* are (*x*-ξ) and *y*, respectively.

$$
\begin{aligned}
d\sigma_x &= \frac{2qd\xi}{\pi}\frac{y(x-\xi)^2}{\left[y^2+(x-\xi)^2\right]^2} \\
d\sigma_y &= \frac{2qd\xi}{\pi}\frac{y^3}{\left[y^2+(x-\xi)^2\right]^2} \\
d\tau_{xy} &= \frac{2qd\xi}{\pi}\frac{y^2(x-\xi)}{\left[y^2+(x-\xi)^2\right]^2}
\end{aligned}
\qquad (1)
$$

By superimposing the stresses induced by each differential concentrated force

ARTICLE IN PRESS

and integrating the above expression over the interval from -*l*/2 to *l*/2, the following equation can be obtained,

$$\begin{aligned}\sigma_x &= \frac{2}{\pi}\int_{-\frac{l}{2}}^{\frac{l}{2}} \frac{qy\left(x-\xi\right)^2 d\xi}{\left[y^2+(x-\xi)^2\right]^2} \\ \sigma_y &= \frac{2}{\pi}\int_{-\frac{l}{2}}^{\frac{l}{2}} \frac{qy^3 d\xi}{\left[y^2+(x-\xi)^2\right]^2} \\ \tau_{xy} &= \frac{2}{\pi}\int_{-\frac{l}{2}}^{\frac{l}{2}} \frac{qy^2\left(x-\xi\right) d\xi}{\left[y^2+(x-\xi)^2\right]^2}\end{aligned} \quad (2)$$

Since the load applied on the top of the coal pillar is simplified as a uniformly distributed load, *q* is treated as a constant. Integrating the above expression yields,

$$\sigma_x = \frac{2}{\pi}\int_{-\frac{l}{2}}^{\frac{l}{2}} \frac{qy\left(x-\xi\right)^2 d\xi}{\left[y^2+(x-\xi)^2\right]^2} = \frac{q}{\pi}\left[\arctan\frac{x+\frac{l}{2}}{y} - \arctan\frac{x-\frac{l}{2}}{y} - \frac{y\left(x+\frac{l}{2}\right)}{y^2+(x+\frac{l}{2})^2} + \frac{y\left(x-\frac{l}{2}\right)}{y^2+(x-\frac{l}{2})^2}\right] \quad (3)$$

$$\sigma_x = \frac{2}{\pi}\int_{-\frac{l}{2}}^{\frac{l}{2}} \frac{qy^3 d\xi}{\left[y^2+(x-\xi)^2\right]^2} = \frac{q}{\pi}\left[\arctan\frac{x+\frac{l}{2}}{y} - \arctan\frac{x-\frac{l}{2}}{y} + \frac{y\left(x+\frac{l}{2}\right)}{y^2+(x+\frac{l}{2})^2} - \frac{y\left(x-\frac{l}{2}\right)}{y^2+(x-\frac{l}{2})^2}\right] \quad (4)$$

$$\tau_{xy} = \frac{2}{\pi}\int_{-\frac{l}{2}}^{\frac{l}{2}} \frac{qy^2(x-\xi)d\xi}{\left[y^2+(x-\xi)^2\right]^2} = \frac{q}{\pi}\left[\frac{y^2}{y^2+(x+\frac{l}{2})^2} - \frac{y^2}{y^2+(x-\frac{l}{2})^2}\right]$$

ARTICLE IN PRESS

It can be observed that the stress state of the strata beneath the floor of the residual coal pillar is primarily governed by the applied load and the position within the floor strata. The stress distribution varies with location beneath the pillar. The influence range of the residual coal pillar on the floor strata increases with increasing depth. The vertical stress directly beneath the coal pillar is the highest, but it decreases progressively with depth. In contrast, the stress in the lateral directions on both sides of the pillar diminishes gradually. As the depth of the floor strata increases, the range of vertical stress influence expands; however, the degree of influence becomes relatively weaker.

3.2 Distribution law of concentrated stress in residual coal pillars

According to the geological and mining conditions of the Yanghuopan Coal Mine, the residual coal pillar between the 20201 and 20202 working faces in the 202 panel

ARTICLE IN PRESS

has a width of 20 m. In this area, the burial depth of the 2^{-2} coal seam is 46 m, including a bedrock thickness of 40 m and an overlying soil layer thickness of 6 m. The caving angle of the bedrock is taken as 58°, while the failure angle of the soil layer is taken as 70°. The average unit weight of the bedrock is 24 kN/m³, and that of the soil layer is 18 kN/m³. Substituting these parameters yields the load borne by the overlying residual coal pillar as q is 2.5 MPa. By substituting q into Eq. (4), the vertical stress distribution in the floor at different depths beneath the residual coal pillar between the 20201 and 20202 working faces in the 202 panel can be obtained. The transmission law of concentrated stress from the residual pillar into the floor is illustrated in Fig. 4.

Based on the analysis in Fig. 4, the concentrated stress transmitted from the residual coal pillar between the 20201 and 20202 working faces in the 202 panel of the Yanghuopan Coal Mine reaches the 3^{-1} coal seam as 0.4 times the applied load (1.0 MPa), located directly beneath the pillar. At this location, the burial depth of the 3^{-1} coal seam is 77m, and the original in-situ stress is calculated as 1.7 MPa. Therefore, under the influence of the concentrated stress induced by the overlying residual coal pillar, the vertical stress borne by the coal seam beneath the pillar prior to the extraction of the 30119 working face is 2.7 MPa, representing a 60% increase compared with the original in-situ stress of 1.7 MPa.

ARTICLE IN PRESS

ARTICLE IN PRESS

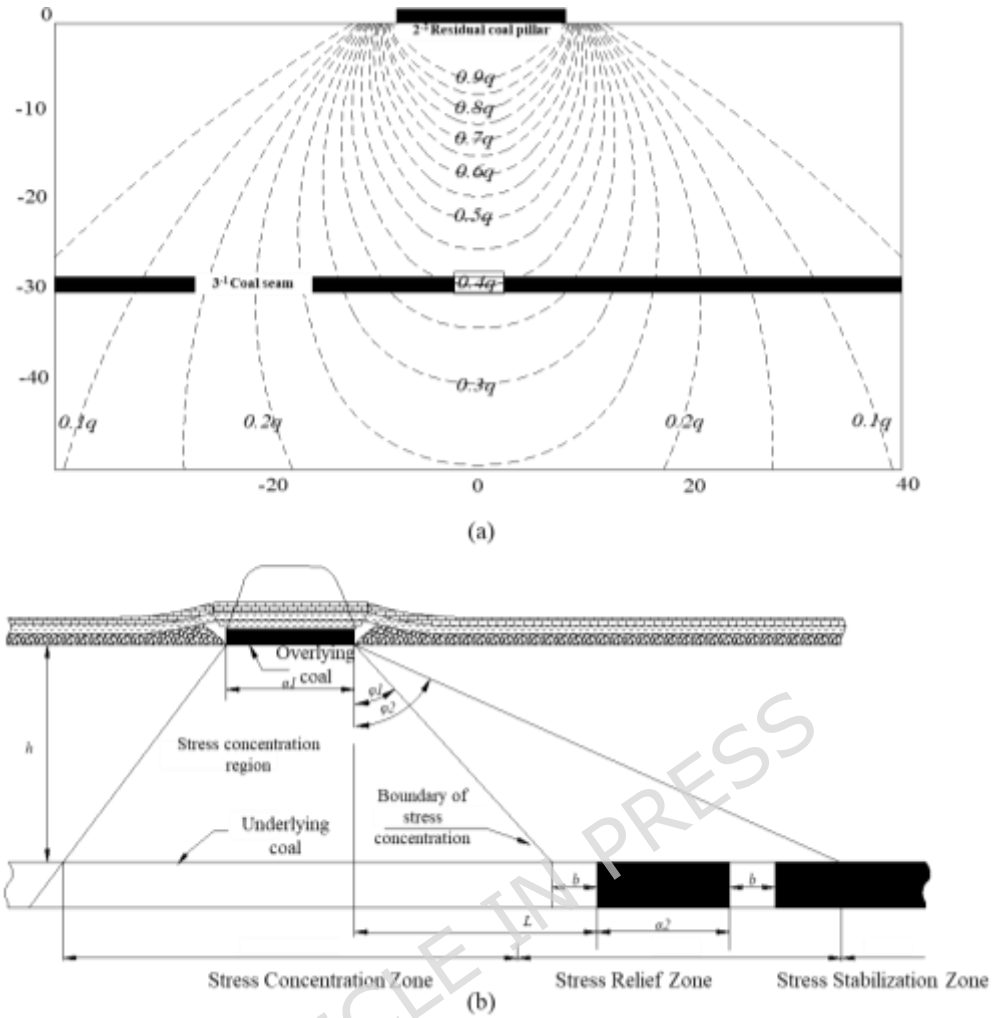


Fig.4 (a) transmission law of concentrated stress from the residual coal pillar to the coal seam floor; (b) stress distribution after the mining of the overlying coal seam.

The residual coal pillars of the upper seam induce stress concentration, relief, and stabilization zones in the underlying floor. According to the caving law of overlying strata, roof breakage propagates upward along a defined fracture angle, lagging behind the advancing face. When the interburden between the upper and lower panels is thin, advance of the lower-seam longwall face at location A precipitates instantaneous failure and caving of the immediate roof along the preconditioned fracture line. The ensuing abutment-stress concentration and overburden load transfer produce a transient escalation in powered-support loading; with continued advance, stress redistribution establishes a stress-relief zone ahead of the face, and the support demand attenuates toward a quasi-steady state (see Fig. 4b).

Based on the above analysis, a mechanical model for concentrated stress transfer

ARTICLE IN PRESS

after upper seam extraction is established, where the influence range of the residual coal pillar on the lower seam can be expressed as:

$$L_{\max} = 2h \tan \varphi_1 + a_1 \tag{5}$$

where, $L_{\max}$ is the maximum range of the concentrated stress from the residual coal pillar in the upper to the lower seam; h is the thickness between the upper and lower seams; a_1 is the width of the residual coal pillar in the upper seam; φ_1 is the maximum influence angle of the concentrated stress from the residual coal pillar in the upper seam. When the residual coal pillar width is 20m and the average seam spacing between the 2^{-2} seam and the 3^{-1} seam is approximately 29 m, and the concentrated stress transmission angle is 36°. Then, the maximum influence range of concentrated stress from the residual coal pillar in the 2^{-2} seam to the 3^{-1} coal seam is 62.1 m.

4 Numerical investigations

4.1 Numerical model

The key to roadways stability in closely spaced coal seams with underlying isolated working faces lies in the stability of the section coal pillar. This work focuses on the stability of the 15m section coal pillar on the return air roadway side of the 30119 working face, and the stability of the return air roadway. Based on aforementioned geological conditions and roadway layout, the FLAC3D software was used to model and analyze the stress distribution in the surrounding rock of the section coal pillar. The model dimensions were 1000 m (length) × 900 m (width) × 180 m (height), with a 100 m boundary coal pillar on both sides along the *x*-direction and y-direction, as shown in Fig. 5. An approximately uniform load is applied to the upper boundary, horizontal constraints are imposed on the vertical boundaries, and the lower boundary is fixed. The Mohr–Coulomb criterion is utilized to model rock failure, and the rock mechanical properties are detailed in Table 2.

ARTICLE IN PRESS

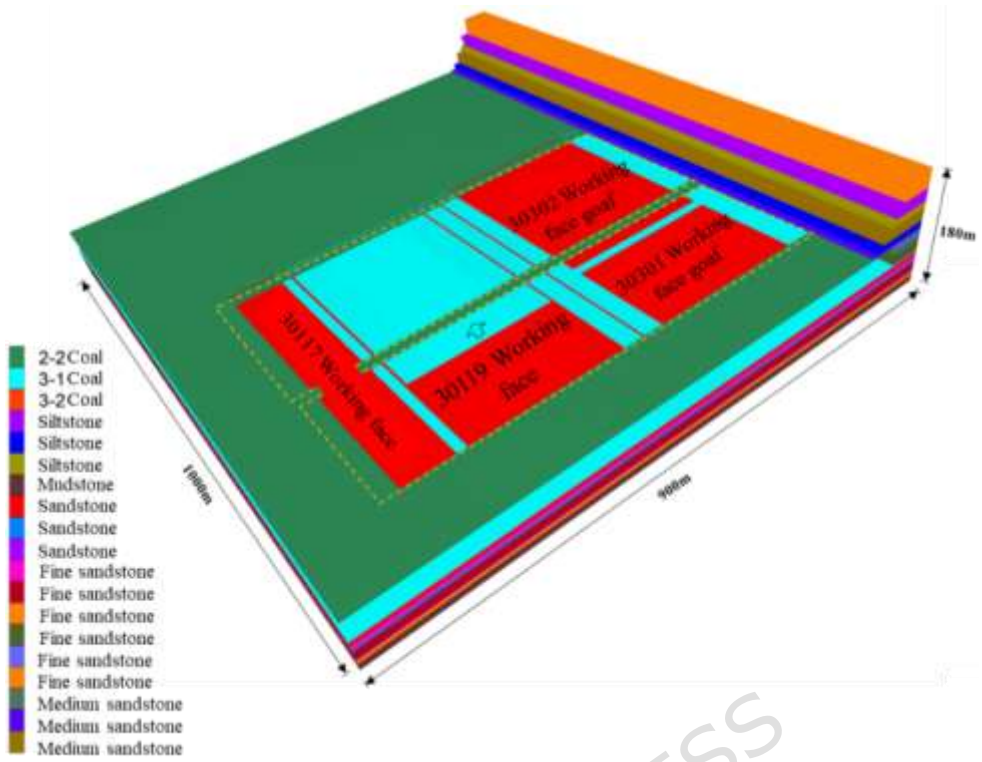


Fig.5 Numerical model of the isolated working face underlying closely spaced coal seams

Table 2 Representative parameters of rock mass.

Rock types	Unit weight /kN·m^{-3}	Tensile strength /MPa	Young's modulus /MPa	Cohesion /MPa	Friction angle/°	Bulk modulus /MPa	Shear modulus /MPa
Soil layer	18.6	0.028	33.42	0.086	30.6	12	37
Sandstone	23.9	1.18	16380	2.2	40.08	6659	10111
Siltstone	24.2	0.62	14830	1.17	39.38	5493	16478
Coal seam	12.9	0.33	6860	0.89	37.01	2618	6018
Siltstone	24	0.98	14260	2.1	38.26	5893	8195
Sandstone	24.3	0.58	11650	1.1	38.25	4447	10219
Siltstone	24.4	1.22	12440	2.29	40.8	4574	14810
Sandstone	24.9	0.78	11150	1.27	40.7	4533	6883
Mudstone	23.5	0.53	13330	1.01	36.28	5375	8545
2^{-2} Coal	12.9	0.33	6860	0.89	37.01	2618	6018
Mudstone	23.5	0.53	13330	1.01	36.28	5375	8545
Sandstone	26.2	1.31	14420	2.4	39.86	6162	7283
Sandstone	24.9	0.78	11150	1.27	40.7	4533	6883
Sandstone	26.2	1.12	14420	2.4	39.86	6162	7283
3^{-1} Coal	12.8	0.48	5240	0.98	36.82	2047	3970

ARTICLE IN PRESS

The purpose of this numerical simulation is to analyze the stability of the 30119 return air roadway and the section coal pillars, particularly focusing on the stress distribution, plastic zone, and displacement variation under the influence of the mining activities in the working face. The mining sequence is as follows. First, the overlying 2^{-2} coal seam is excavated, forming the mined-out areas of the 20201 and 20202 working faces, as well as 1# and 2# residual coal pillars, as shown in Fig. 6a. Subsequently, the 3^{-1} coal seam is extracted. During the extraction of the 3^{-1} coal seam, the mined-out areas on both sides and the three entryways of the 30119 working face are extracted, resulting in the unexcavated conditions of the 30119 working face, as illustrated in Fig. 6b. Owing to the spatial configuration of the 30119 working face, which is oriented perpendicular to the 20201 and 20202 working faces within the 3^{-1} coal seam, the completion of upper-seam extraction induces a well-defined redistribution of concentrated stresses, resulting in the formation of five distinct stress transfer zones. From the mine boundary toward the interior, these zones are sequentially characterized as follows: (1) a stress-relief region beneath the 20201 working face, (2) a concentrated stress domain governed by residual coal pillar 1, (3) a stress-relief region beneath the 20202 working face, (4) a concentrated stress domain associated with 2# residual coal pillar, and (5) the original in-situ stress zone beneath the unmined 2^{-2} coal seam, as depicted in Fig. 6c.

As illustrated in Fig. 6d, before the extraction of the 30119 working face, the vertical stress at the 0 m position exhibits a gradual attenuation, primarily controlled by the boundary effect of the overlying 2^{-2} coal seam pillar. Beneath the 1# residual coal pillar, the stress field develops in a distinctly symmetrical manner, with the maximum value of 13.12 MPa concentrated directly below the pillar centerline. By contrast, the stress distribution beneath the 2# residual coal pillar is characterized by an abrupt increase followed by a progressive reduction, reaching a peak of 7.26 MPa, which is approximately 45% lower than that beneath the 1# pillar. This pronounced disparity demonstrates that the abutment stresses induced by the adjacent goafs of the 20201 and 20202 working faces superimpose in a coupled manner, thereby amplifying the concentrated loading on the 1# residual coal pillar. Consequently, the

ARTICLE IN PRESS

vertical stress beneath the 1# pillar is nearly double that beneath the 2# pillar, revealing a highly heterogeneous redistribution of concentrated stresses that governs the mechanical response of the underlying strata under close-distance coal seam mining conditions.

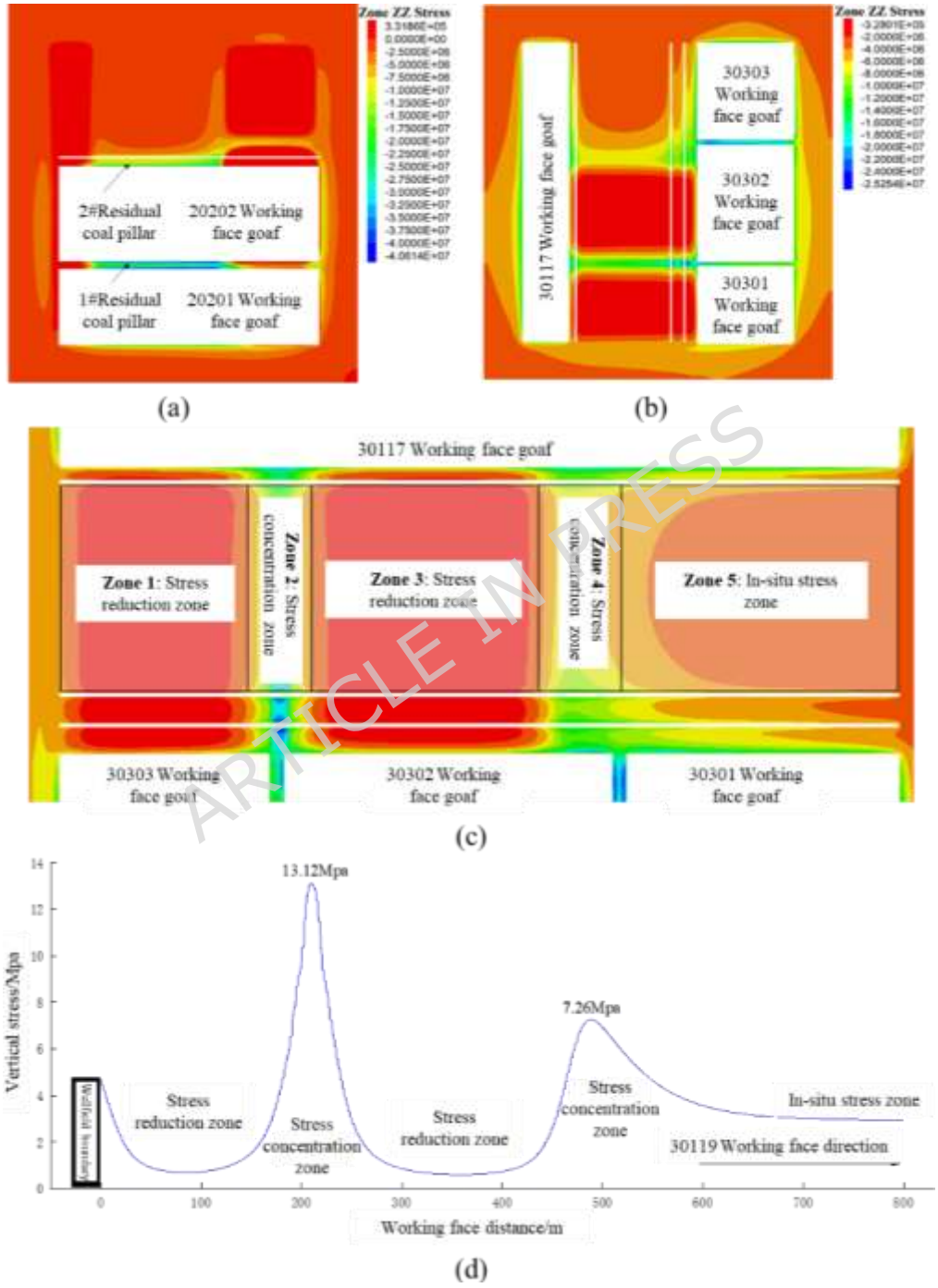


Fig.6 Stress analysis before 30119 working face extraction: (a) and (b) vertical stress distribution; (c) five distinct stress transfer zones of the 2^{-2} coal seam; (d) vertical stress distribution in the floor of the 2^{-2} coal seam

ARTICLE IN PRESS

4.2 Stability analysis of the return air roadway during 30119 working face excavation

Numerical simulations were conducted to investigate the plastic zone in the surrounding rock and the vertical stress distribution along the 30119 return air roadway before excavation of the 30119 working face (see Fig. 7). The results indicate that, under the influence of a residual coal pillar, the vertical stress in the coal pillar segment and along the roadway sidewalls is significantly higher directly beneath regions 2 and 4. In contrast, the stress concentration observed directly beneath regions 1 and 3 is relatively low. Beneath region 5, the stress concentration is greater than that in regions 1 and 3 but remains lower than that in regions 2 and 4. Furthermore, simulation results show that when the plastic zone of the surrounding rock is situated beneath a residual coal pillar, the plastic zone along the 30119 return air roadway sidewalls expands compared to the results where the roadway is located in regions 1 and 3.

ARTICLE IN PRESS

ARTICLE IN PRESS

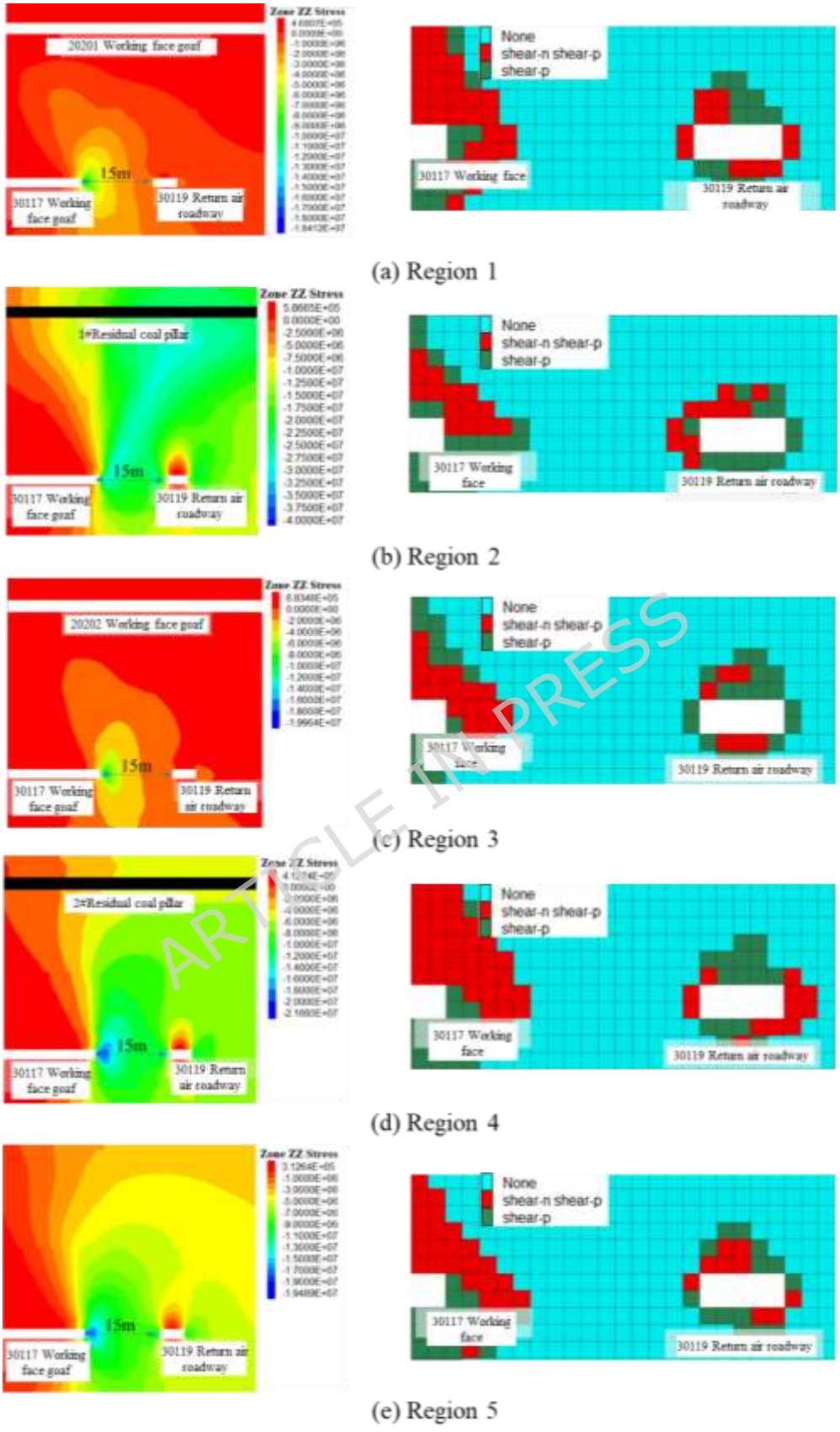


Fig.7 Analysis of surrounding-rock and sectional coal pillars in five regions before 30119 working face extraction

ARTICLE IN PRESS

Based on the stress distributions delineated for the five regions, numerical simulations were performed to resolve the stage-dependent evolution of the advanced abutment pressure (AAP) during the extraction of working face 30119. Fig. 8 and 9 present the spatial stress fields of the five regions and the corresponding AAP profiles for each mining stage. The AAP attained a peak at approximately 8 m ahead of the face in phase 1, with an average peak of 3.26 MPa. In phase 2, the peak AAP increased markedly. However, a pronounced decline occurred once the face advanced beyond the residual coal pillar. In phases 3,4, and 5, the AAP again appeared at 8 m, with maximum stress at 6.30 MPa, 17.18 MPa, and 16.83 MPa, respectively. Overall, the simulations indicate a consistent localization of the AAP peak at 8 m ahead of the face and a strong sensitivity of its magnitude to the presence and subsequent removal of the residual pillar, with the most pronounced stress concentration occurring in phases 4 and 5.

ARTICLE IN PRESS

ARTICLE IN PRESS

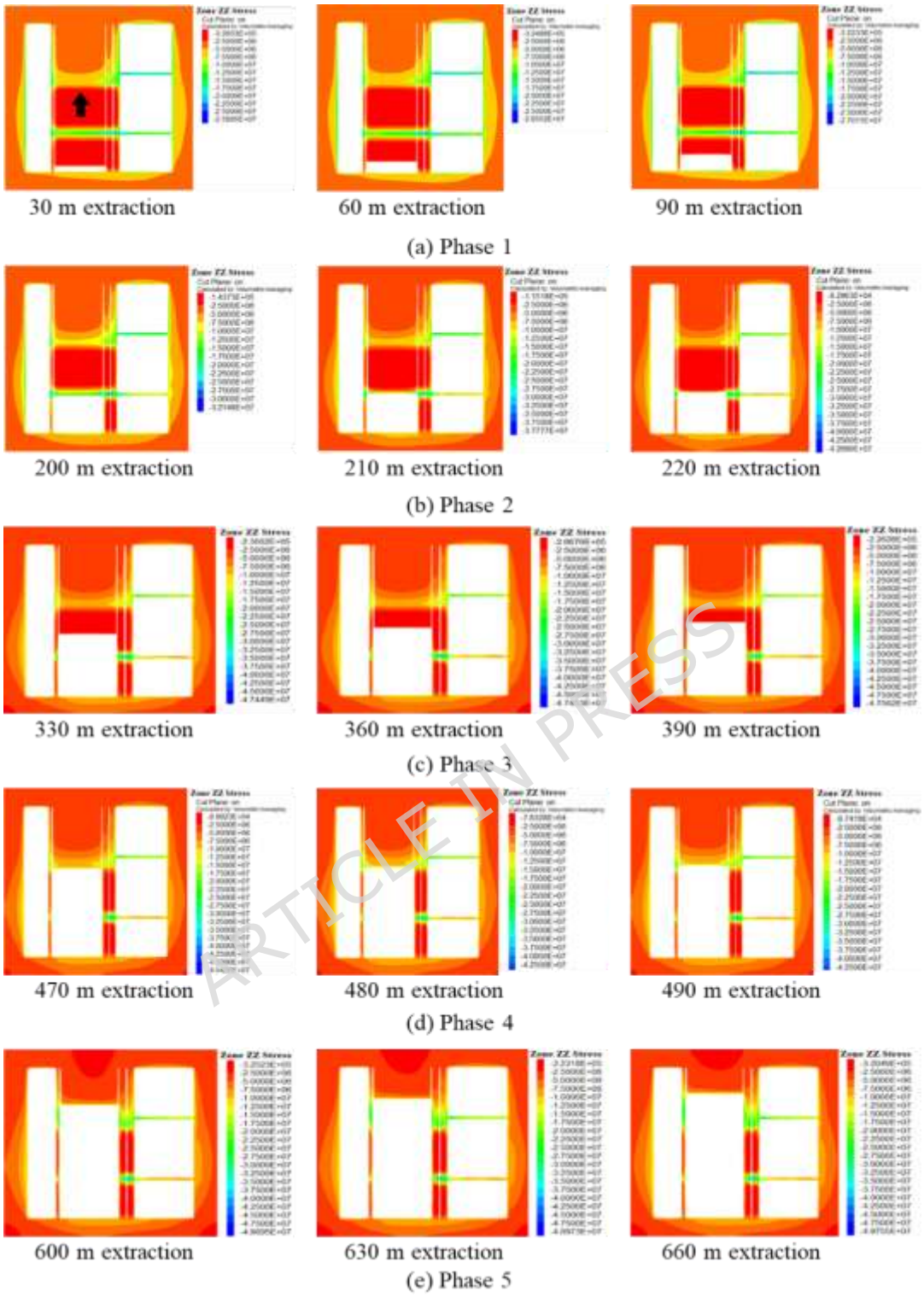


Fig.8 Stress distribution across five phases in 30119 panel.

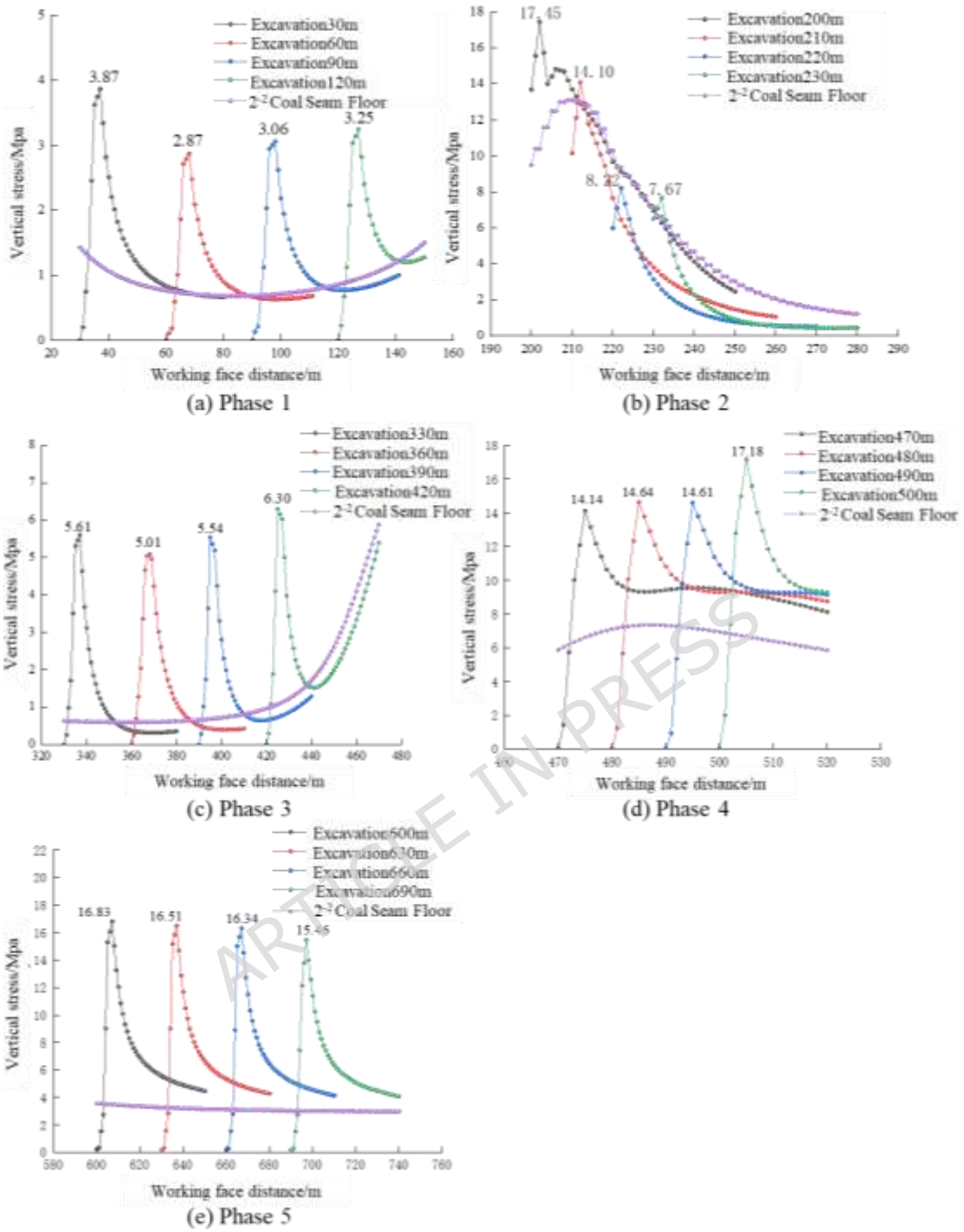


Fig.9 Vertical stress distribution at different phases of the 30119 panel.

To investigate the effect of different mining phases on the vertical stress and plastic zone evolution in the sectional coal pillar, numerical simulations were conducted with measurement points every 5m. As shown in Fig. 10a, in the first phase, the vertical stress distribution inside the coal pillar ahead of the face exhibited a double-peak pattern since this region lay within a stress-relief zone under the floor of

ARTICLE IN PRESS

the overlying 2^{-2} coal seam. As a result, the stress peak was higher on the side adjacent to the 30117 working face and lower near the 30119 return air roadway. Under the influence of advance support loads, the sidewalls and roof experienced plastic deformation, with the maximum plastic depth reaching 2 m in the sidewall and up to 3 m in the roof (see Fig. 11a). In the second stage, influenced by an overlying residual coal pillar, the pillar's stress profile became saddle-shaped, and the influence of the advance support loads diminished with distance (Fig. 10b). As depicted in Fig. 10b, under the combined effects of the residual pillar and the advance support loads, the roadway deformation was more severe, and the roof plastic zone height reached 5 m, and the sidewall plastic zone depth reached 3 m. In the third phase, the stress distribution again exhibited a double-peak pattern at the face advance, with the 30117 working face side remaining relatively high and the 30119 return air roadway side lower (Fig. 10c). Since the pillar was still partly in the stress-relief zone of the 2^{-2} coal seam floor. As depicted in Fig. 11c, the induced plastic zones were 2 m in the sidewalls and 3 m in the roof. By the fourth stage at a 500 m advance (see Fig. 10d), the stress peaks of pillars clearly diminished with distance at 20 m ahead of the face. The advance support loads produced plastic zones of 3 m depth in the sidewalls and 4 m in the roof (see Fig. 11d). In the fifth phase, the vertical stress of coal pillar decreased uniformly with distance (see Fig. 10e). At 5 m, 10 m, and 20 m ahead of the face in the 30119 return air roadway, the advance support loads caused plastic zones of approximately 2 m in the sidewalls and 3 m in the roof (see Fig. 11e).

ARTICLE IN PRESS

ARTICLE IN PRESS

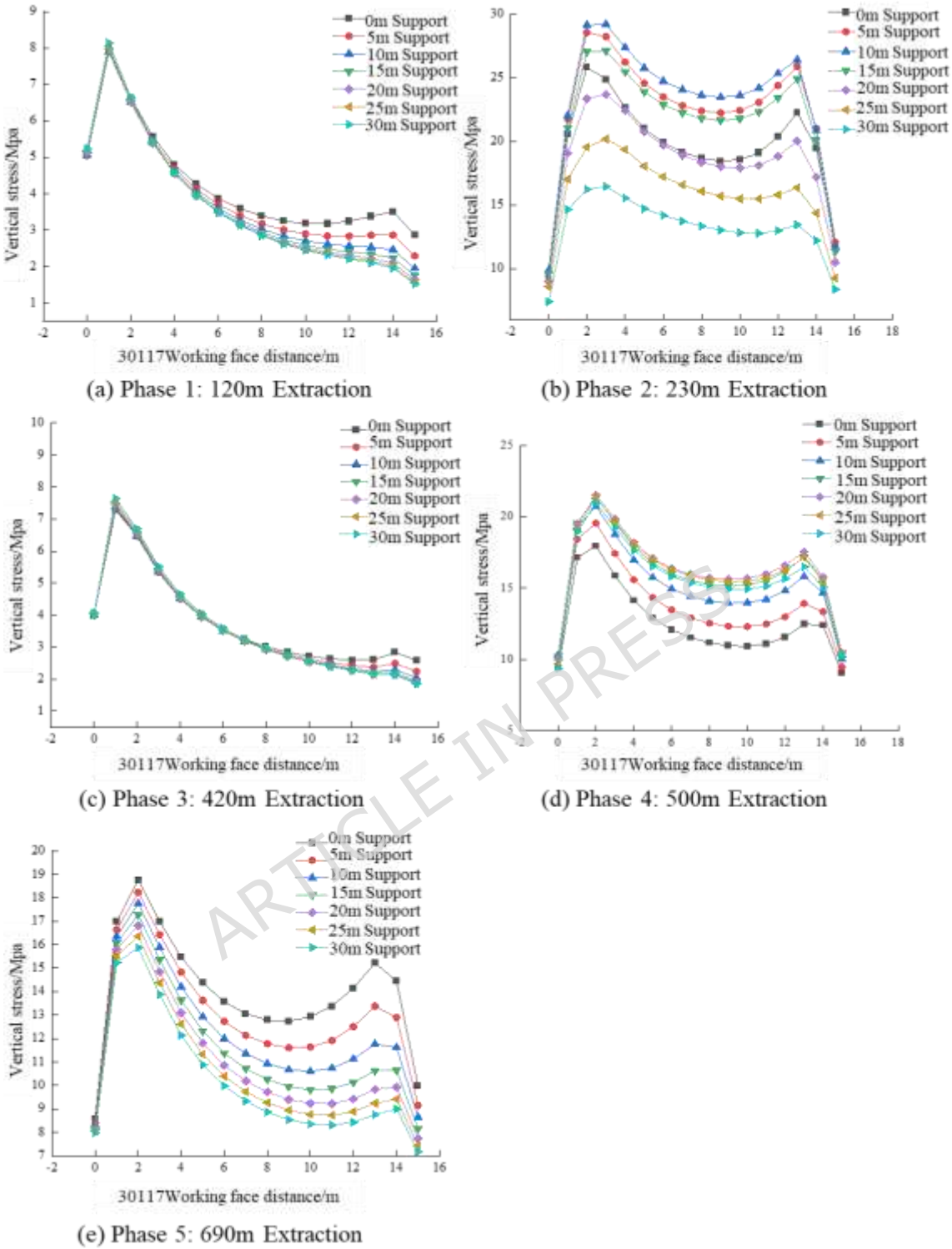
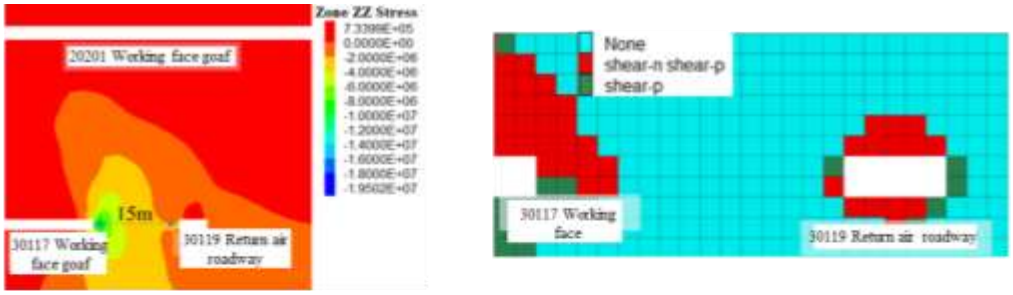
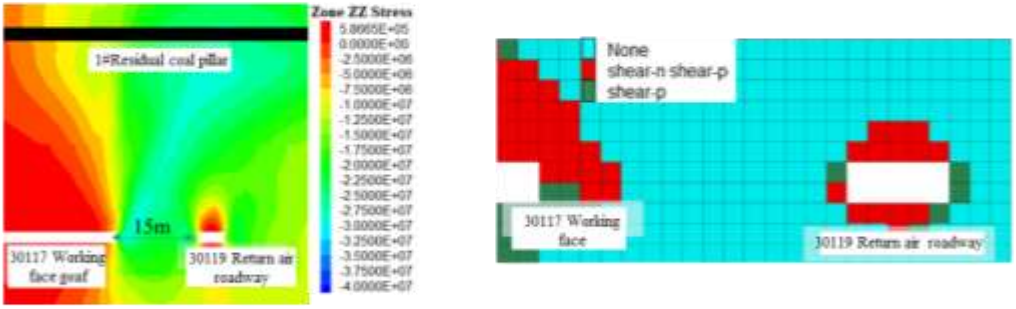


Fig.10 Vertical stress of the sectional coal pillar during 30119 working face extraction in different phases.



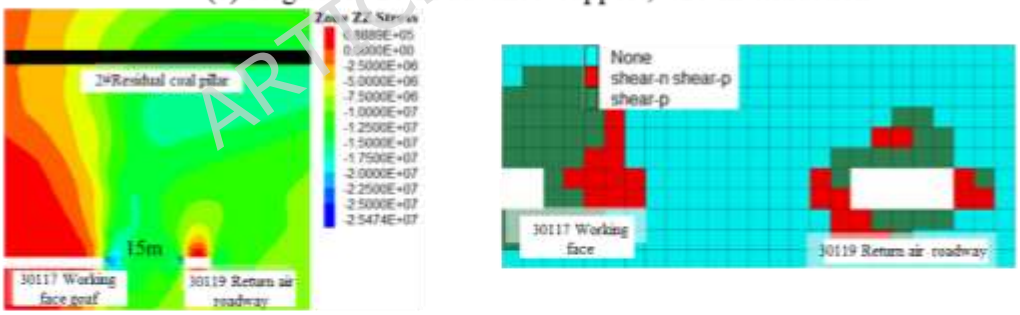
(a) Region 1: 20m advance support, 120 m extraction



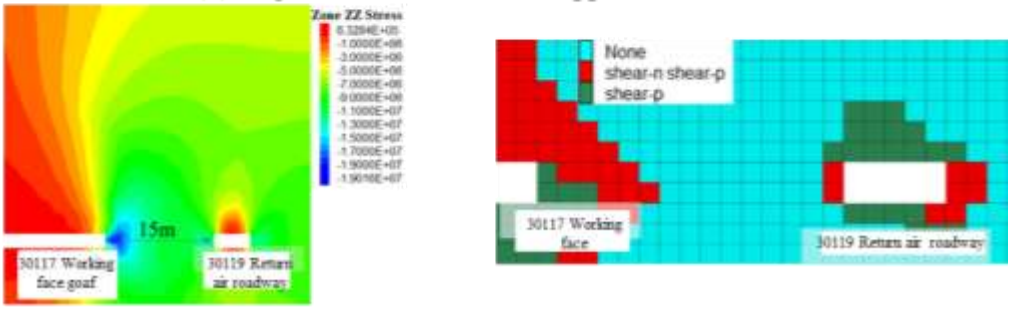
(b) Region 2: 20 m advance support, 230 m extraction



(c) Region 3: 20 m advance support, 420 m extraction



(d) Region 4: 20 m advance support, 500 m extraction



(e) Region 5: 20 m advance support, 690 m extraction

Fig.11 Plastic zones evolution of surrounding rock and coal pillars across five regions during extraction of the 30119 panel.

ARTICLE IN PRESS

To investigate the deformation of the surrounding rock in the return air roadway of the 30119 working face, measurements were taken at multiple advance stages (Fig. 12). Phase 1 showed a maximum displacement of 42 mm at the sidewall and 22.5 mm at the coal pillar sidewall, while roof displacement steadily decreased from 34.7 mm to 1.1 mm (Fig. 12a). In Phase 2, the roof displacement decreased from 209.6 mm to near 0 mm; the coal sidewall displacement declined from 96.5 mm to 60.9 mm before gradually increasing to 65.1 mm, and the coal pillar sidewall displacement increased gradually (Fig. 12b). Phase 3 presented the roof displacement drop from 30.1 mm to nearly 0 mm and then rise to 48.2 mm. The coal sidewall displacement declined from 39.4 mm to 14.6 mm; and the coal pillar sidewall displacement decreased from 23.2 mm to near 0 mm (Fig. 12c). Phase 4 showed the roof displacement falling from 354.3 mm to 261.9 mm; the coal sidewall displacement initially declined from 57.8 mm to near 0 mm before slowly increasing to 29.3 mm; and the coal pillar sidewall displacement increased from 60.2 mm to 63.9 mm and then stabilized (Fig. 12d). Finally, in Phase 5, the roof displacement decreased from 219.9 mm to 127.8 mm; the coal sidewall displacement fell from 36.8 mm to near 0 mm and then rose to 25.0 mm; and the coal pillar sidewall displacement increased from 29.5 mm to 36.3 mm and then remained essentially constant (Fig. 12e).

ARTICLE IN PRESS

ARTICLE IN PRESS

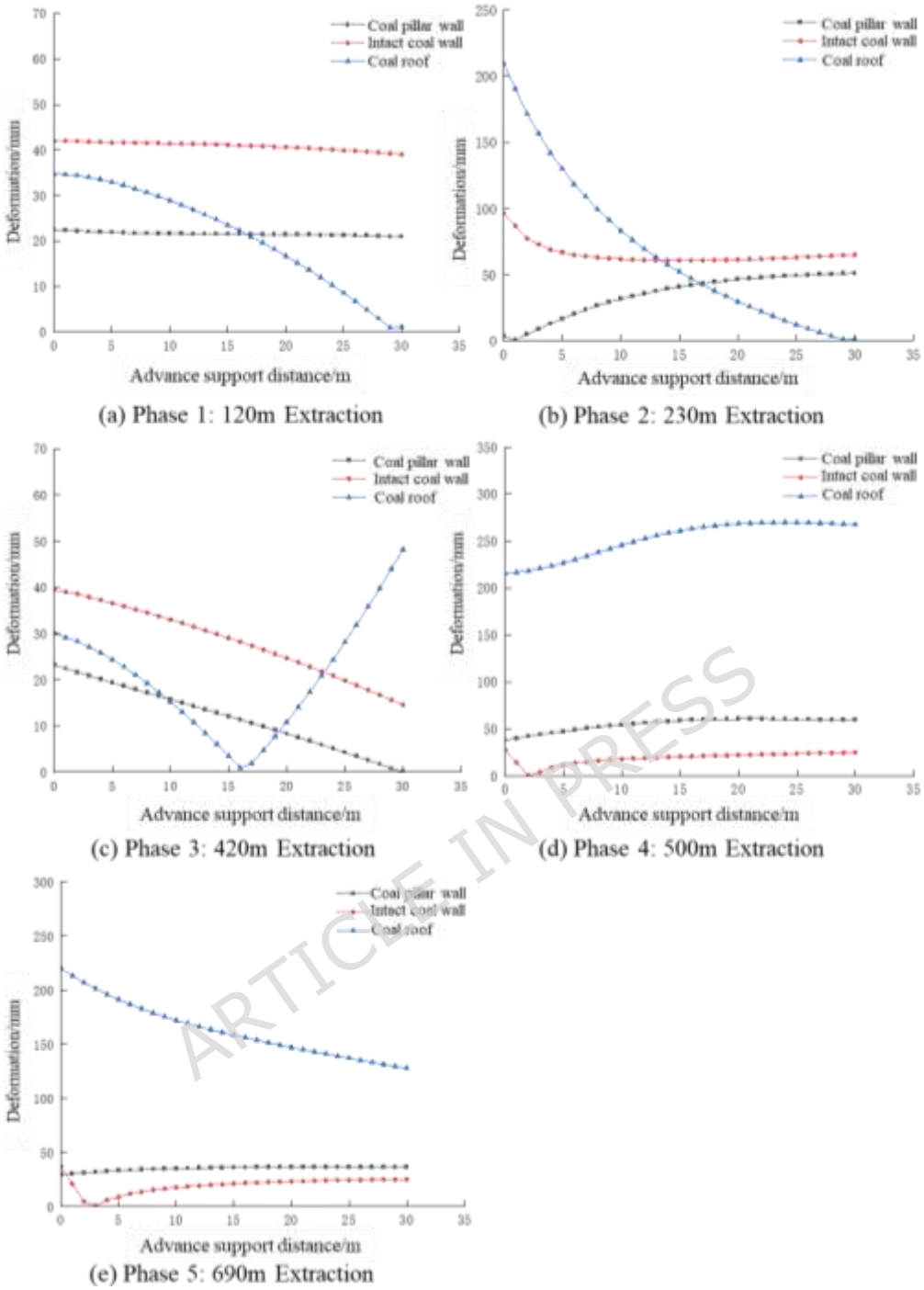


Fig.12 Surrounding rock deformation of the return air roadway at different extraction phases.

5 Proposed support technology

5.1 Control scheme of segmental surrounding rock support.

For the 30119 panel in Yanghuopan coal mine, a zoned ground-control strategy is formulated to ensure roadway stability during the retreat of the isolated longwall. The return air roadway is partitioned into: (1) a conventional-support zone, comprising the

ARTICLE IN PRESS

60 m destressed belt beneath the overlying goaf and the adjacent in-situ stress domain, and (2) an enhanced-support zone, directly under overlying remnant pillars where stress concentration is elevated (see Fig. 13a). Roof control employs integrated bolt–mesh/strap–cable bolting system with ϕ20×2000mm rebar bolts at 1.0 m×1.0 m with bolt lines 0.6 m from each sidewall, and ϕ15.24×6300 mm cable bolts in a "2–1–2" array at 2.0 m×3.0 m, with cable lines 1.6 m from sidewall. Owing to the low rib-side stress concentration in the easy and in-situ domains, dedicated rib reinforcement may be omitted there; the sectional layout is shown in Fig. 13b.

Given the isolated-panel geometry of the 30119 working face (0–1150 m) and the superposed abutment from the overlying 2^{-2} coal seam residual pillar, an enhanced-support zone is prescribed for the affected reach. Roof reinforcement adopts a composite system-fully grouted ϕ20×2000mm rebar bolts at 1.0 m×1.0 m with bolt lines 0.6 m from each sidewall, supplemented by ϕ15.24×6300 mm cable bolts in a "2–1–2" array at 2.0 m×3.0m and 1.6 m sidewall offset—integrated with welded wire mesh/steel straps. Rib confinement follows the principles of shoulder-angle control and pillar integrity: ϕ20×2000mm rebar bolts at 1.0 m×1.0 m, positioned 0.5 m below the roof line and 0.9 m above the floor (see Fig. 13c). This specification targets reduced convergence, delayed plastic-zone coalescence, and enhanced entry stability under the superposed static–dynamic stress regime characteristic of isolated-panel retreat.

ARTICLE IN PRESS

ARTICLE IN PRESS

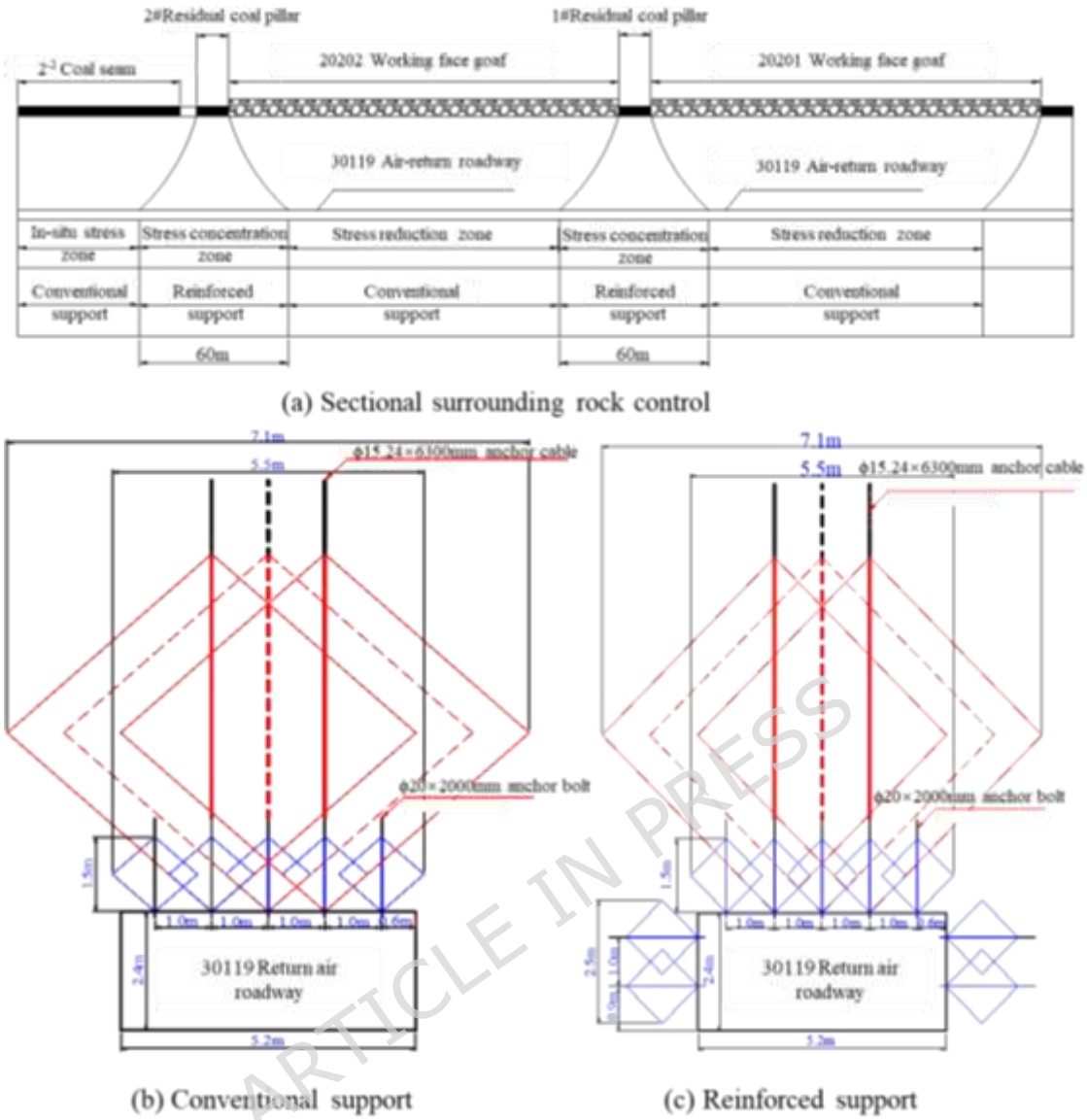


Fig.13 Combined control scheme for the surrounding rock in the 30119 panel.

To evaluate the adequacy and reliability of the initial support design, a comprehensive monitoring program was implemented in the 30119 return air roadway. The monitoring system incorporated surface and deep displacement measurements of surrounding rock, as well as real-time load assessment of bolts and cables, to provide an integrated evaluation of roadway stability. Data were systematically collected during the extraction process, enabling validation of support performance and timely assessment of deformation mechanisms. It should be noted that the monitoring work was initiated after roadway excavation and reinforcement. To ensure representativeness, monitoring stations were strategically positioned in geologically continuous sections of the roadway. Three stations, designated K1, K2, and K3, were

ARTICLE IN PRESS

deployed at 50 m intervals, thereby ensuring spatial coverage of stress redistribution effects. The monitoring framework and station configuration are presented in Fig. 14.

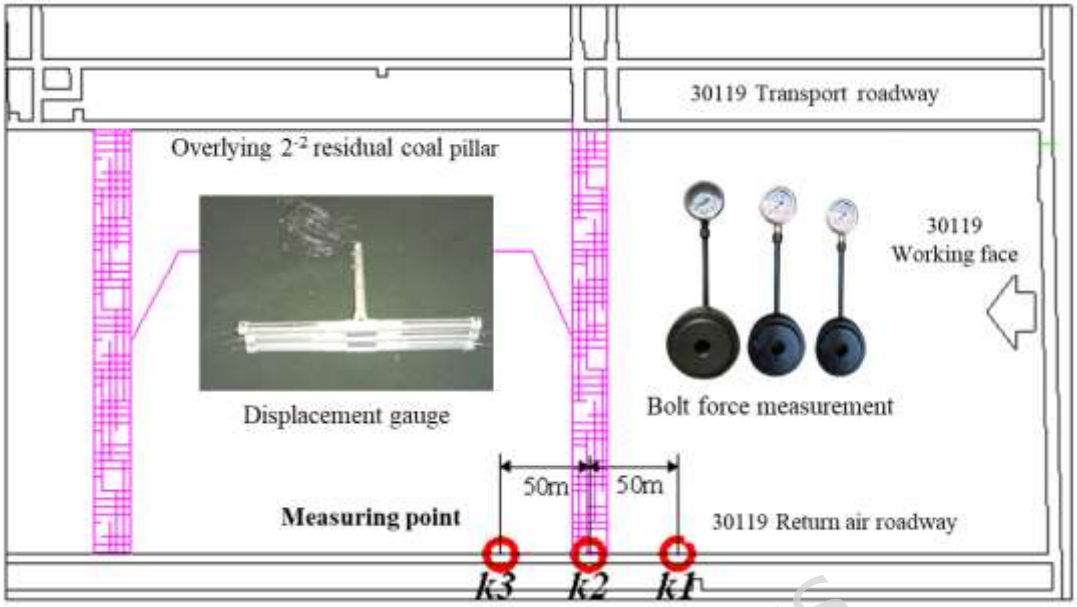


Fig.14 Layout of rock mass deformation monitoring stations in the roadway.

5.2 Analysis of in-situ monitoring results for roadway deformation during mining excavation

To quantify the roadway surface deformation, the monitoring program primarily focused on the sidewall convergence and roof subsidence of the 30119 return air roadway. Based on in-situ measurements, the temporal–spatial evolution of relative displacement and deformation velocity was analyzed to determine the ultimate deformation of the surrounding rock and to evaluate the effectiveness of the support system. Following reinforcement, three monitoring stations (K1, K2, K3) were installed, and a 30-day observation campaign was conducted to characterize roof deformation. As shown in Fig. 15, results indicate that roof subsidence initiated approximately 60 m ahead of the working face, remaining nearly constant until 25 m, where the roadway was only affected by minor stress perturbations rather than the advanced abutment pressure. Beyond 25 m ahead of the face, roof subsidence increased significantly, entering the influence zone of the advanced abutment pressure, with a maximum subsidence rate of 1 mm/d. The effective influence range of advanced abutment pressure was thus determined to be 25 m. During the monitoring period, the maximum recorded roof subsidence was 10 mm, indicating that the

ARTICLE IN PRESS

existing support scheme effectively controlled roof deformation and ensured the safe and stable operation of the working face.

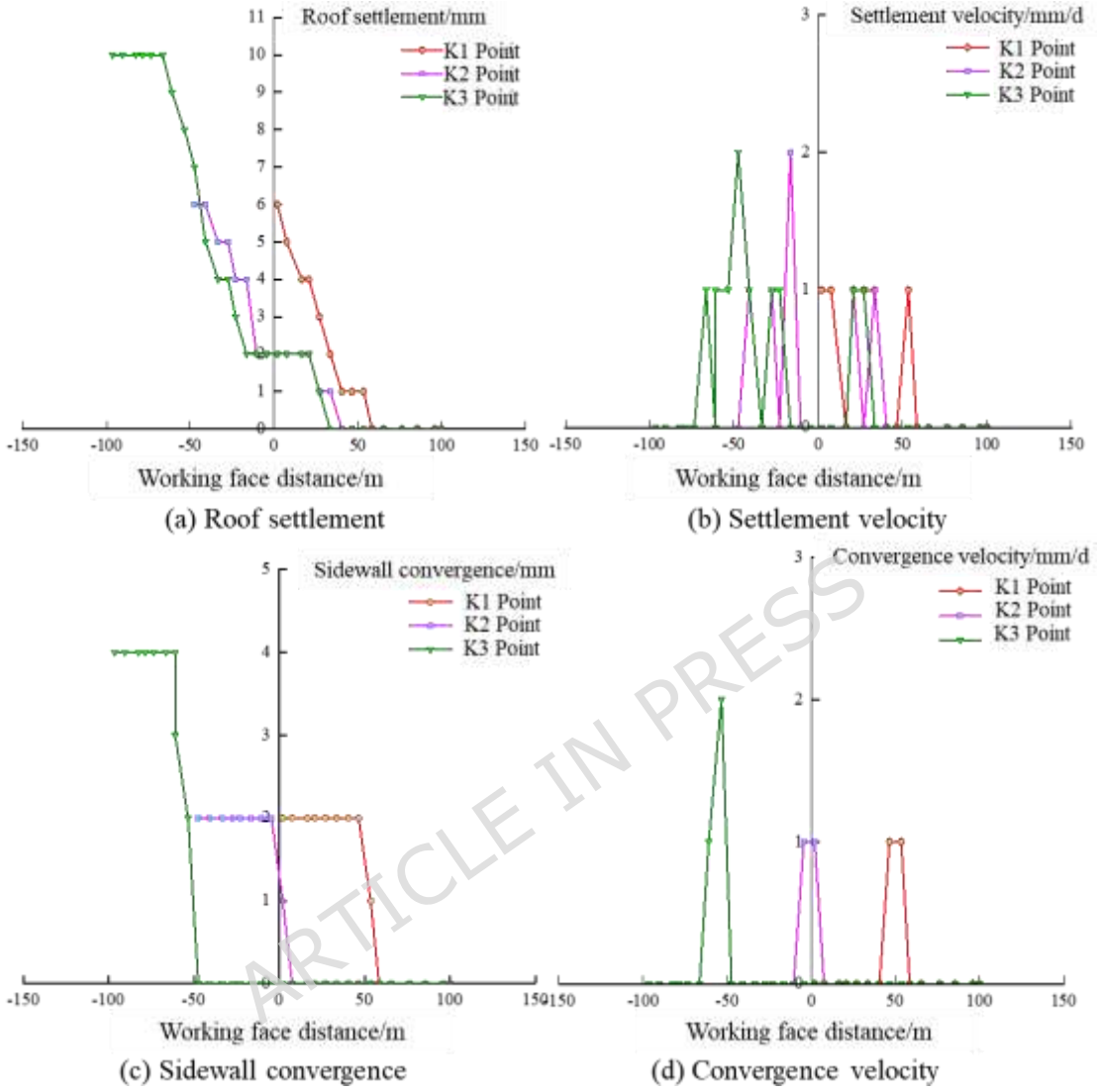


Fig.15 Roof settlement and velocity curves for the return air roadway of 30119 working face.

As shown in Fig. 16, deformation at the coal-pillar sidewall is highly confined. Within the bolt–grout anchorage zone (0-2.0 m), relative displacement is effectively zero; a narrow transition band with 2 m to 3 m exhibits the peak relative movement, after which horizontal displacement from 3.0 to 6.0 m again approaches zero. The maximum lateral offset of the pillar rib is 2 mm. The small amplitudes and tight spatial confinement of displacement collectively demonstrate that the implemented bolt–mesh–cable support scheme affords robust confinement and a high stability margin of the reinforced rock mass.

ARTICLE IN PRESS

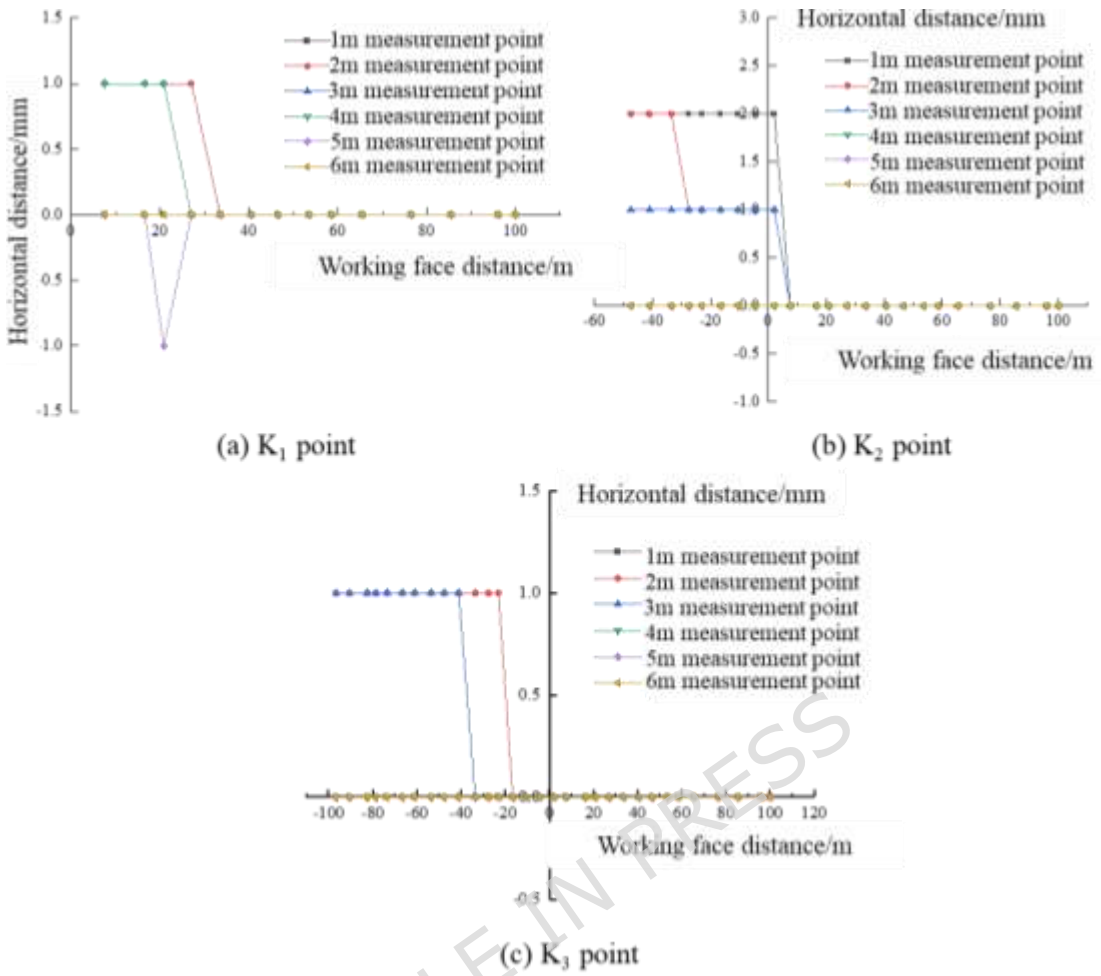


Fig.16 Monitoring deformation of surrounding rock at different monitoring stations.

To characterize reinforcement demand with face advance, instrumented rebar bolts and strand-type cable bolts were deployed at stations K1 to K3 on the extraction-side rib, roof, and pillar-side rib of the 30119 return air roadway (Fig. 17). The monitoring delineates an advanced abutment-stress influence zone of 40 m along the pillar-side rib and 30 m at the roof. The interval from the face to 100 m behind constitutes an overburden adjustment zone. Peak axial loads were 28 kN (solid-coal rib bolts), 40 kN (roof bolts), and 38 kN (chain-pillar rib bolts), against a 105 kN rated yield for Φ 20 mm left-hand-thread deformed rebar bolts. Cable-bolt demand peaked at 78 kN on the chain-pillar rib, i.e., 0.30 of the 260 kN yield for Φ17.8 mm 1×7 steel strand. All demands are well within capacity, evidencing sufficient reserve and corroborating the effectiveness of the composite bolt–mesh/strap–cable support system.

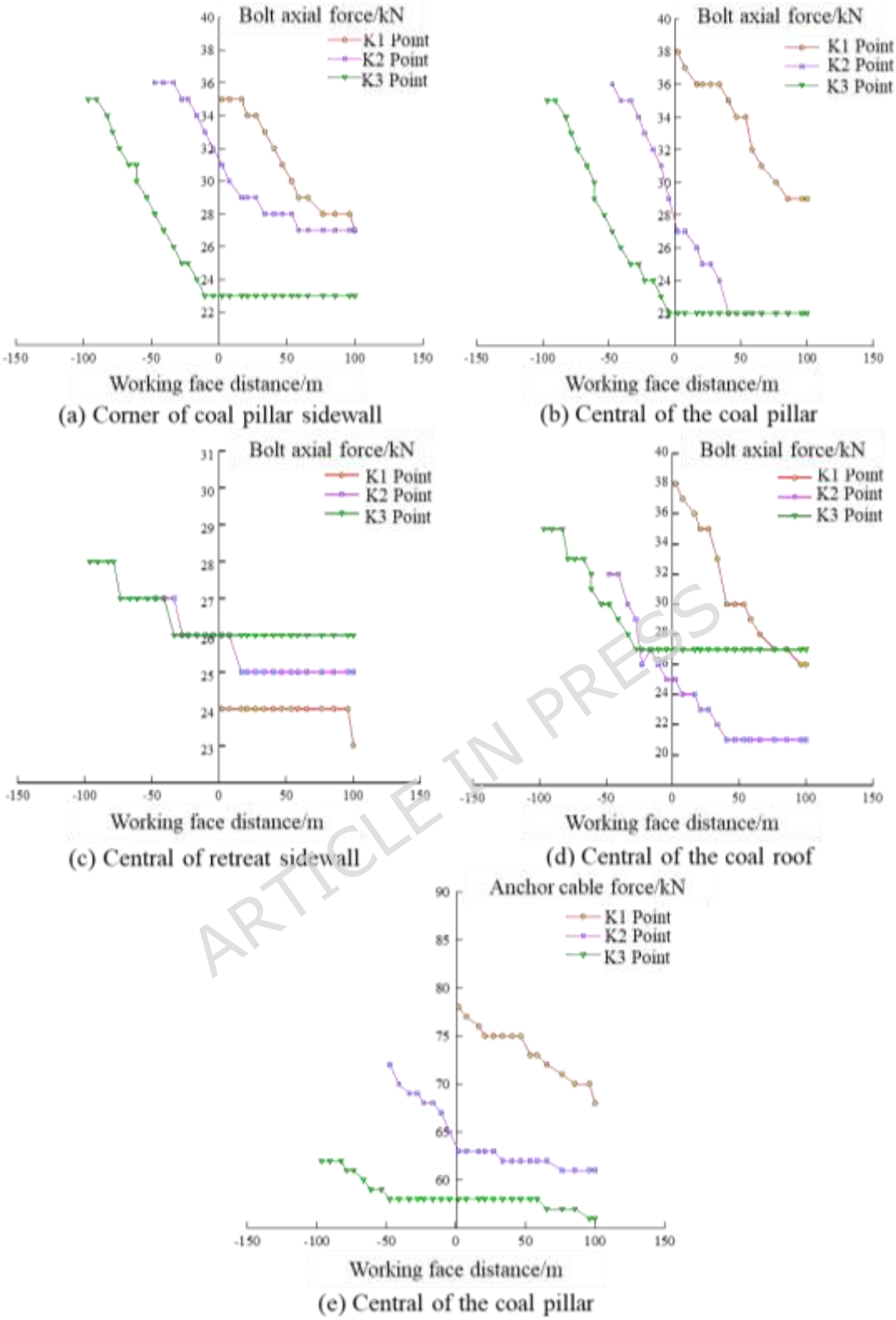


Fig.17 Axial force evolution of rock bolts and cable bolts at different monitoring stations

6 Conclusions

The deformation and stability of roadways in the underlying isolated island

ARTICLE IN PRESS

working face were investigated through theoretical analysis, numerical modelling and field observations at the Yanghuopan coal mine. The deformation characteristics of the roadway surrounding rocks during 30119 panel excavation were analyzed systematically, and the corresponding stability control schemes were proposed. The main conclusions are as follows:

(1) The mining of the underlying isolated island working face is influenced by the combined effects of stress from the mined-out area and the overlying residual coal pillar. Through analysis, it is determined that the vertical stress in the 3^{-1} coal seam at the location of the residual coal pillar is 1.6 times greater than the original in-situ stress, with the stress impact extending over a distance of 62.1 m. Utilizing limit equilibrium theory and incorporating the stress transfer mechanism in the 2^{-2} coal seam.

(2) Numerical analysis of the surrounding rock stress and plastic zone failure in the 30119 return air roadway reveals distinct deformation and stress patterns across different mining areas. The peak advanced support pressure beneath the 1# residual coal pillar reaches 17.18 MPa. The sectional coal pillar stress exhibits a double-peak distribution beneath the residual coal pillars, with vertical stress beneath the 1# residual coal pillar being 28.3% higher than that beneath the second. Additionally, deformation of the roof and solid coal sidewall beneath the 2# residual coal pillar is significantly reduced, with roof deformation decreasing by 50% and solid coal sidewall deformation by 76.3%, while coal pillar sidewall deformation remains similar.

(3) In the 30119 working face, surrounding rock control is categorized into strengthened and conventional support zones based on the stress environment and rock fracturing conditions of the return air roadway. The strengthened support sections, influenced by overlying residual coal pillars, utilize ϕ20×2000mm threaded steel bolts with 1000×1000mm spacing for side support. In contrast, the conventional support zone, located beneath the mined-out area and above the underlying coal seam, employs ϕ20×2000mm bolts and ϕ15.24×6300mm anchor cables arranged in a “2-1-2” triaxial pattern with 2000×3000 mm spacing.

ARTICLE IN PRESS

(4) Field observations have demonstrated that the maximum roof subsidence in the strengthened support section of the 30119 return air roadway is 10mm, while the maximum sidewall convergence is 4mm. The support bolts and cables for both the sidewalls and roof are subjected to the relatively substantial residual bearing capacity of the 30119 working face. Monitoring results show that the combined support scheme can effectively control roadway deformation, which can provide guidance for controlling the stability of the underlying isolated island working face with similar conditions. However, due to safety and installation constraints, the monitoring data captures only a limited short-term response, and more comprehensive real-time sensing, the development of advanced constitutive models, and economic benefits comparisons will be required in future works.

CRediT authorship contribution statement

Xiaoxu Gao: Conceptualization, Supervision. Yaowei Wang: Data curation, Writing. Yi-Ming Li: Conceptualization, Data curation, Writing-original draft.

Declaration of Competing Interest

The authors declare that they have no known competing financial interests or personal relationships that could have appeared to influence the work reported in this paper.

Data availability statement

The datasets used during the current study available from the corresponding author on reasonable request.

Funding

This work was supported by the National Natural Science Foundation of China Youth Project (Grant No. 52404141), China Postdoctoral Science Foundation (Grant No. 2024MD753978), and project by the Guangdong Provincial Key Laboratory of Deep Earth Sciences and Geothermal Energy Exploitation and Utilization (Grant No. DESGEEU-2024-01).

ARTICLE IN PRESS

References

1. Zhang, S., Wang, X., Fan, G., Zhang, D., & Cui Jianbin. Pillar size optimization design of isolated island panel gob-side entry driving in deep inclined coal seam-case study of Pingmei No. 6 coal seam. *JOURNAL OF GEOPHYSICS AND ENGINEERING* **15**, 816–828 (2018).
2. Wen, Y. *et al.* Strata Movement and Mining-Induced Stress Identification for an Isolated Working Face Surrounded by Two Goafs. *ENERGIES* **16**, (2023).
3. Wang, T. *et al.* Impact hazard analysis of islanding face mining based on micro-seismic monitoring and shock wave CT inversion. *Journal of Geophysics and Engineering* **22**, 520–531 (2025).
4. Liu, G., Mu, Z., Chen, J., Yang, J. & Cao, J. Rock burst risk in an island longwall coal face by stress field. *Geosci J* **22**, 609–622 (2018).
5. Wang, W., Wu, Y., Shi, Y. & Zhu, J. Outburst mechanism and hazard prevention technique of limestone aquifer under isolated island panels. *FRONTIERS IN EARTH SCIENCE* **12**, (2025).
6. Li, M. *et al.* Failure mechanism and control technology of soft-rock roadways subjected to high structural stress. *Front. Earth Sci.* **12**, 1473108 (2024).
7. Liu, H. *et al.* Study on the Law of Mine Pressure Manifestation in Three-Soft Coal Seam Isolated Working Face. *APPLIED SCIENCES-BASEL* **15**, (2025).
8. Hao, Y. *et al.* Analysis of Stress and Deformation on Surrounding Rock Mass of a Trapezoidal Roadway in a Large Inclination Coal Seam and Novel High Yielding Prop Support: A Case Study. *Mathematics* **11**, 319 (2023).
9. Jia, C. *et al.* Mining Pressure Distribution Law and Disaster Prevention of Isolated Island Working Face Under the Condition of Hard 'Umbrella Arch'. *ROCK MECHANICS AND ROCK ENGINEERING* **57**, 8323–8341 (2024).
10. Li, Y.-M. *et al.* A benchmark study of different numerical methods for predicting rock failure. *International Journal of Rock Mechanics and Mining Sciences* **166**, 105381 (2023).
11. Wang, Y., Chen, P. & Wang, S. Study of Overlying Rock Structure and Intensive Pressure Control Technology of Island Longwall Panel in Extra-Thick Coal Seams. *PROCESSES* **11**, (2023).
12. Shang, Y. *et al.* Study on Failure Characteristics and Control Technology of Roadway Surrounding Rock under Repeated Mining in Close-Distance Coal Seam. *Mathematics* **10**, 2166 (2022).
13. Xie, J., Xu, J. & Wang, F. Mining-induced stress distribution of the working face in a kilometer-deep coal mine—a case study in Tangshan coal mine. *J. Geophys. Eng.* **15**, 2060–2070 (2018).
14. Meng, N., Bai, J. & Yoo, C. Failure mechanism and control technology of deep soft-rock roadways: Numerical simulation and field study. *Underground Space* **12**, 1–17 (2023).
15. Yang, W. *et al.* Research on Reasonable Width of Coal Pillars of Non-equal Width Isolated Working Face Heading Goaf in Deep Mine. *GEOTECHNICAL AND GEOLOGICAL*

ARTICLE IN PRESS

ENGINEERING **40**, 1295–1306 (2022).

16. Xue, B. *et al.* Optimisation research on a thin coal seam isolated island coal face mining back channel layout and its support parameters. *INTERNATIONAL JOURNAL OF OIL GAS AND COAL TECHNOLOGY* **31**, 297–315 (2022).
17. Li, Y.-M., Li, J.-L., Wu, Y. & Zhao, G.-F. Extracting Rock Parameters Through Digital Drilling Test. *Rock Mechanics and Rock Engineering* **57**, 8215–8241 (2024).
18. Khan, A., Li, Y., Shoaib, M., Sajjad, U. & Rui, F. Utilizing machine learning and digital twin technology for rock parameter estimation from drilling data. *Journal of Intelligent Construction* **3**, 9180088 (2025).
19. Li, Y.-M. & Zhao, G.-F. A numerical integrated approach for the estimation of the uniaxial compression strength of rock from point load tests. *International Journal of Rock Mechanics and Mining Sciences* **148**, 104939 (2021).
20. Chen, Q., Zuo, Y. & Zheng, L. Deformation failure mechanism and stability-control technology of deep layered clastic-rock roadway under dynamic disturbance. *TUNNELLING AND UNDERGROUND SPACE TECHNOLOGY* **156**, (2025).
21. Huang, D. *et al.* Influence of strength inhomogeneity on transboundary expansion characteristics of hydraulically fractured fractures in coal seams. *Scientific Reports* **14**, 29094 (2024).
22. Ni, H. *et al.* Effect of mining-induced abutment pressure on gateroad and grouting-based bolting technology: A case study. *ENGINEERING FAILURE ANALYSIS* **151**, (2023).
23. Bai, J. *et al.* Evolution Laws of Stress-Energy and Progressive Damage Mechanisms of Surrounding Rock Induced by Mining Disturbance. *APPLIED SCIENCES-BASEL* **13**, (2023).
24. Lu, A. *et al.* Analysis of rockburst hazard and optimization of prevention and control measures in multi-seam mining based on refined numerical simulations. *BULLETIN OF ENGINEERING GEOLOGY AND THE ENVIRONMENT* **84**, (2025).
25. Han, C., Yang, H., Zhang, N., Deng, R. & Guo, Y. Zoning Control Technology of Gob-Side Roadway Driving with Small Coal Pillar Facing Mining in a Special Isolated Island Working Face: A Case Study. *APPLIED SCIENCES-BASEL* **11**, (2021).
26. Huang, W., Jing, G., Ma, L., Zhao, L. & Wang, S. Research on blasting technology for thick and hard roof fracturing in isolated island coal mine working face. *SCIENTIFIC REPORTS* **15**, (2025).
27. Lin, H. *et al.* Study on the Energy Evolution Mechanism and Fractal Characteristics of Coal Failure under Dynamic Loading. *ACS Omega* **10**, 54710–54719 (2025).
28. Sun, B., Liu, S., Zeng, S., Wang, S. & Wang, S. Dynamic characteristics and fractal representations of crack propagation of rock with different fissures under multiple impact loadings. *Scientific Reports* **11**, 13071 (2021).
29. Zou, P., Fan, H., Liu, H., Jin, K. & Zhong, H. Experimental study on energy evolution and damage characteristics of unloading coal under cyclic loading. *Scientific Reports* **15**, 16630 (2025).

ARTICLE IN PRESS

ARTICLE IN PRESS

30. Zhang, C., Ji, H., Fu, Z. & Zhang, Y. Analysis of fracture characteristics and energy evolution of tectonic coal after loading based on acoustic emission. *Measurement* **252**, 117388 (2025).

ARTICLE IN PRESS